

Article

# Effectiveness of Sacrificial Shielding for Blast Mitigation of Steel Floating pontoons

Yasser A. Khalifa<sup>1,2</sup>, Mohamed N. Lotfy<sup>1,2,\*</sup> and Elsayed Fathallah<sup>2,3,\*</sup> 

<sup>1</sup> Civil Engineering Department, McMaster University, Hamilton, ON L8S 4L8, Canada

<sup>2</sup> Department of Civil Engineering, Military Technical College, Cairo 11865, Egypt

<sup>3</sup> Ships and Submarines Engineering Department, Military Technical College, Cairo 11835, Egypt

\* Correspondence: lotfym@mcmaster.ca (M.N.L.); saidhabib2000@hotmail.com or saidhabib2000@mtc.edu.eg (E.F.)

**Abstract:** Floating pontoons have played a supreme and indispensable role in crises and disasters for both civil and military purposes. Floating bridges and ferries are exposed to blast loadings in the case of wars or terrorist attacks. The protection effectiveness of sacrificial cladding subjected to a blast was numerically investigated. In this study, a steel ferry has been simulated and exposed to side explosions with different explosive charges at certain stand-off distances, according to military standards from NATO and American standard TM5. In this simulation, nonlinear three-dimensional hydro-code numerical simulation ANSYS autodyn-3d has been used. The results reported that the ferry could withstand a charge of 5 kg TNT at a stand-off distance of 1 m without failure. The main objective of this research is to achieve a design that would increase the capacity against the blast loading with minimal plastic deformation in the absence of any failure in the ferry. Therefore, an innovative mitigation system has been proposed to dissipate the blast energy of the explosion based on the scientific theory of impedance using sacrificial cladding. The new mitigation system used a specific structural system in order to install the existing pontoon structure without any distraction. The response, elastic deformations, plastic deformations and plastic failure of the ferry were illustrated in this paper. Furthermore, the results revealed that the proposed mitigation system could mitigate more than 50% of the blast waves. The new design revealed promising results, which makes it suitable for mitigating blast waves. Finally, the results were provided with a reference for the preliminary design and application of sacrificial cladding for structural protection against blast waves.

**Keywords:** floating; pontoon; AUTODYN; blast; mitigation; modeling; plastic deformation



**Citation:** Khalifa, Y.A.; Lotfy, M.N.; Fathallah, E. Effectiveness of Sacrificial Shielding for Blast Mitigation of Steel Floating Pontoons. *J. Mar. Sci. Eng.* **2023**, *11*, 96. <https://doi.org/10.3390/jmse11010096>

Academic Editors: Bin Liu, Kun Liu and Chenfeng Li

Received: 5 December 2022

Revised: 25 December 2022

Accepted: 27 December 2022

Published: 4 January 2023



**Copyright:** © 2023 by the authors. Licensee MDPI, Basel, Switzerland. This article is an open access article distributed under the terms and conditions of the Creative Commons Attribution (CC BY) license (<https://creativecommons.org/licenses/by/4.0/>).

## 1. Introduction

Due to accidental explosions and increasing terrorist attacks, preventive and blast-resistant techniques are needed to ensure the survivability of structures. The development of new technologies to protect structures against explosions has gained significant attention, not only for military applications but also for civilian purposes. Any design of the blast load mitigation system must incorporate influence on the mitigation efficiency and the study of attenuation mechanisms.

Techniques of protection against explosion dangers and various mitigation strategies have recently attracted the attention of many researchers [1–9]. Liu et al. [10] investigated the blast load attenuation of sandwich panels. The results demonstrated that sandwich panels could reduce the peak load by 64.69% compared with mild steel plates without a foam core. Cheng et al. [11] studied the effect of cladding sandwich panels subjected to blast loading with different configurations of tubular cores. The results illustrated that cladding panels could be used as an option for blast mitigation. Chen et al. [12] designed sandwich panels with layered-gradient aluminum foam cores subjected to blast loading.

The results illustrated that the layered-gradient sandwich panel has advantages in terms of blast resistance and energy absorption. Wang et al. [13] presented a numerical method to simulate a rocket explosion on a launch pad to study the propagation law of near-ground explosions and quantify the enhancement effect on peak overpressure. Zhou and Hao [14] demonstrated that a protective barrier could effectively reduce blast loading and protect the structures from explosion effects. Furthermore, Abdel Wahab et al. [15] presented a protection system to protect vehicles from blast effects. Alqwasmi et al. [16] studied the behavior of sacrificial sandwich steel panels with axially oriented octagonal tapered tubular cores subjected to blast loading. Additionally, it was found that the top plate and tube thickness are significantly affected by energy absorption. Additionally, Alogla et al. [17] designed protective panels to segregate building façades from the effect of an explosion. The robust design demonstrated great performance, not only in resisting the blast waves but also in providing protection against fragments. Markose and Lakshmana [18] explored a composite plate with V-shaped steel plates and coatings of hyperplastic materials, such as polyurea, to enhance blast mitigation. Moreover, Moustafa et al. [19] developed a novel blast load mitigation system employed as a protection fence, using a bent tube technique to manipulate the shockwave. The results showed that this technique could mitigate 94% of the blast waves, which means that only 6% of the blast impulse is considered an applied load on the targeted structure.

Additionally, Jin et al. [20] proposed different configurations for steel poles used as a fence for a building in order to enhance its protection by mitigating the pressure wave. As an alternative blast mitigation method, sacrificial cladding has attracted attention in recent years [21]. Sacrificial cladding generally consists of a core sandwiched with one or two face plates [22,23]. With the aid of sacrificial cladding, the load transmitted to the structure can be significantly reduced [24]. However, further investigations are still needed to provide more convincing predictions regarding the blast mitigation effectiveness of sacrificial cladding. Yasser A. Khalifa et al. [22] studied the performance of lightweight, cold-formed steel sandwich panels subjected to explosions, as well as energy absorption and scalability. The results suggested that panels with a unidirectional core configuration are preferable to mitigating blast risk. Hong yuan Zhou et al. [21] presented an experimental and numerical investigation to study the effectiveness of using a sacrificial cladding consisting of a steel face plate and an aluminum foam core for near-field blast mitigation. Additionally, Zhang et al. [25] studied the dynamic response of corrugated sandwich structures with different core arrangements to maximize the mitigation effects of blasts. Britan et al. [26] investigated the possibility of using foam materials with high deformability and energy absorption capacity in sacrificial lightweight blast walls. Taha et al. [27] studied the effect of using ultra-high-performance concrete in curved concrete barrier walls to capture the damage produced due to blast explosions. The results illustrated that using ultra-high-performance concrete in barrier walls has a good influence on mitigating the effect of blast explosions, with an average percentage of 32% compared to ordinary concrete barriers. Ehasni et al. [28] incorporated composite materials for protection against an explosive charge of 100 kg of TNT. Furthermore, McDonald et al. [29] experimentally studied the dynamic responses of high-strength and armor-grade steel subjected to explosions at different stand-off distances. Guangyong et al. [30] investigated the effect of the face-sheet configuration and materials on the blast resistance of a structure constructed from sandwich panels. Zong et al. [31] used fence walls for blast wave distraction and investigated their mitigation capabilities. The results showed that the fence walls could reduce the peak pressure and impulse. Moreover, Xia et al. [32] numerically investigated the protective performance of metallic foam cladding on a reinforced concrete slab. Wu and Sheikh [33] studied the influence of metallic foam cladding on protecting a concrete slab subjected to an explosion. Yazici et al. [34] determined the dynamic responses of a sandwich panel against blast loading. The results showed that the deflections were decreased by 50%, and the weight of the panel decreased by approximately 2.3%. Abdel Wahab et al. [35] and Markose and Rao [18] established a mitigation system (V-shape) for protecting the hull of a military

vehicle subjected to an explosion. Marcel et al. [36] numerically investigated the effect of the core topologies of sandwich-structured composites in terms of dynamic responses, failure mechanisms and energy absorption. The results clarified that comparable structural characteristics could be achieved by changing the external dimensions and shapes and also by changing the core density. Lin et al. [37] designed and compared sandwich panels with different types of honeycomb cores to construct an optimized blast wall on an offshore platform. The results clarified that the sandwich plate with a concave arc honeycomb core had the best anti-blast performance.

Based on the previous studies, further investigations are needed to provide more convincing predictions about blast mitigation effectiveness. In the present study, the protective effects of sacrificial cladding were proposed. Three-dimensional numerical simulations using commercial finite element ANSYS AUTODYN have been performed to develop a blast load mitigation system that can be used as a fence to satisfy acceptable protection for a floating steel ferry. The model has first been validated using previous experimental tests. The validation process was based on a real experiment and a series of practical experiments performed by Aune et al. [38]. In addition, a new mitigation system has been proposed and simulated to attenuate the generated blast wave and significantly reduce its effect.

### 1.1. Blast Loading

An explosion is a very rapid release of an enormous amount of energy in a very short time accompanied by an air pressure shock wave [39,40]. This air pressure shock wave compresses the surrounding air and then decays after reaching the peak according to the type, stand-off distance and the charge mass of the explosive [41]. The pressure profiles and equivalents can be determined from Hopkinson–Cranz scaling laws, where the pressure and stand-off distance are expressed as variables of the Hopkinson scaled distance ( $Z$ ), as in Equation (1) [42–45].

$$Z = R/W^{1/3} \tag{1}$$

where “ $R$ ” represents the stand-off distance (meter), and “ $W$ ” represents TNT equivalent charge mass (kg). The blast load depends on the explosive material and the basis of its physical state [46]. Explosions are classified as far-range explosions when the offset distance is equal to or greater than  $1.2 \text{ m/kg}^{1/3}$ , and near-range explosions are when the offset distance is less than  $1.2 \text{ m/kg}^{1/3}$ . The typical pressure–time history, which results from air explosions, is analyzed and illustrated in Figure 1 [17,47–50].

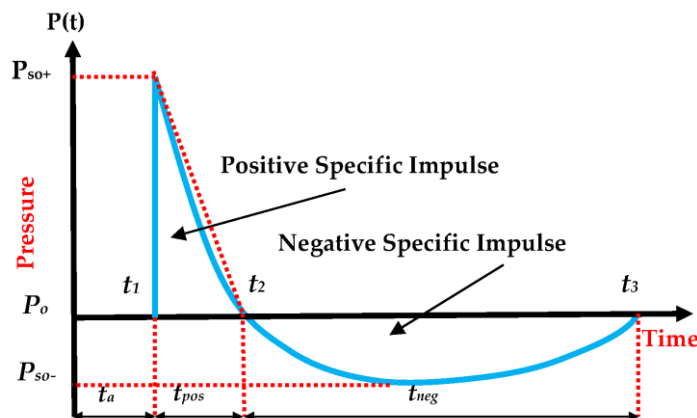


Figure 1. Typical pressure-time history from air explosions [17,47–50].

This curve represents the change in the pressure versus time at any location away from the center of the explosion. Where “ $P_{SO}$ ” represents the peak incident pressure, “ $P_o$ ” represents the ambient atmospheric pressure, “ $P_{SO}^-$ ” represents the negative pressure and “ $t_a$ ” is the arrival time. The blast wave reaches the structure according to the stand-off

distance and the charge mass at the time equal to “ $t_a$ ”, and at this point, the pressure reaches its maximum and is equal to ( $P_{SO}$ ). After that, the incident pressure decreases until it reaches atmospheric pressure. The elapsed time that the blast wave takes from the peak pressure to reach the atmospheric pressure is known as the positive phase duration ( $t_O$ ). This is followed by a negative pressure called the negative phase duration ( $t_O^-$ ). The incident impulse (i) is the integrated area under the pressure–time history curve. The pressure can be calculated at any time according to Equation (2) [17,51].

$$P(t) = P_O + P_{SO} (1 - t/t_O) e^{-\mu(t/t_O)} \tag{2}$$

where  $P(t)$  represents the pressure at any time “ $t$ ”, “ $\mu$ ” represents the pressure wave decay parameter, “ $P_{SO}$ ” represents the peak incident pressure and “ $P_O$ ” represents the ambient atmospheric pressure.

### 1.2. Strain Rate Effect

The response of the materials varies according to the type of loading. The blast and impulsive loads affect the structures with a very high velocity. The very rapid influence in a short period of time with high energy causes the nonlinearity behavior of the materials. The materials that are exposed to such high impulsive loads generate high strain rates up to ( $10^6 \text{ s}^{-1}$ ) [52]. This strain rate affects the strength of the materials; therefore, the simulation of these materials requires a proper understanding of the strain rate effect. Many efforts have been devoted to understanding the strain rate influence since 1960 [52–54]. Zener and Hollomon [55] concluded that most engineering structures were only affected by the strain rate in their elastic ranges, and this follows the elastic zone of the stress–strain curves, which is because of the slow loading rate of static loads. The responses of those structures have changed from the elastic zone to the plastic zone for the blast loads, affecting the high strain rate. This effect is a result of the very short duration of loading (impulse loading). Due to the importance of the strain rate in problems where plastic deformations are expected to appear, the strain rate effect must be considered in impulsive loading problems [55,56]. The Taylor impact test was performed to determine the plasticity parameters at high strain rates (up to  $10^5 \text{ s}^{-1}$ ) for metals [57]. Koerber et al. [58] presented an experimental investigation of the influence of the strain rate on unidirectional carbon-epoxy characteristics, such as mechanical properties and failure strength. It was concluded that the compressive failure strain is not the strain rate sensitive to the studied strain rates.

The Johnson–Cook equation is one of the most important material models used to determine the dynamic response of materials under a high strain rate of order  $10^3 \text{ s}^{-1}$  or higher [4,59]. This model is used to represent the strength behavior of materials, typically metals that are subjected to large strains, high strain rates and high temperatures. Such behavior might arise in problems of intense, impulsive loading due to high-velocity impact. In addition, the yield stress in this model varies depending on the strain, strain rate and temperature. Equation (3) illustrates the Johnson–Cook equation [59,60].

$$\sigma = [A + B \times \epsilon_p^n][1 + C \times \ln \epsilon^*][1 - T_H^m] \tag{3}$$

$$\epsilon^* = \frac{\epsilon}{\epsilon_0} \tag{4}$$

where “ $\sigma$ ” represents the material strength, “ $\epsilon_p^n$ ” represents the effective plastic strain, “ $\epsilon^*$ ” is the dimensionless plastic strain for  $\epsilon_0 = 1$ , “ $T_H^m$ ” represents the temperature material softening and  $A, B, C, n$ , and  $m$  are five constants that depend on the characteristics of the used material [59] and are defined as follows [61–64]: Constant “ $A$ ” represents the yield stress corresponding to an offset strain value of 0.2%, constant “ $B$ ” and exponent “ $n$ ” represents the effect of the material strain hardening, and constant “ $C$ ” represents the strain rate effect. The Johnson–Cook model is represented by three terms that affect the strength of materials; the first one represents the relationship between the stress and the strain, the second represents the relationship between the stress and the strain rate while

the last one represents the temperature effect on stress during plastic deformation. The proper simulation of any material in AUTODYN depends upon the definition of the used parameters according to the used equation of state, strength and failure equations.

## 2. Problem Explanation and Numerical Modeling

Floating bridges are very important for both civilian and military purposes [65,66]. For military usage, blast loadings have a disastrous effect on the floating ferry in the present design. Altering the design of the floating ferry requires replacing the whole number of floating pontoons already used. This problem can be solved by the implementation of an additional structure with specific characteristics to dissipate the explosive energy.

### 2.1. Problem Description and Methodology

The objective is to mitigate the explosion's energy to facilitate floating steel ferry/bridge operation in hazardous scenarios. For military purposes, standards and manuals (e.g., NATO Standards [67,68] and American Standards [69]) determine the levels of protection and the possible charges of several water mines. The innovative system has a simple internal configuration that can be attached to existing floating pontoons (no need to manufacture new pontoons). The simulation was performed using ANSYS AUTODYN. The reduction in the transmitted pressure waves depends on the mechanical impedance ( $I$ ) of the medium [70], which is defined as the ratio between the change in the pressure ( $\Delta p$ ) to the change in the velocity of the shock wave ( $\Delta v$ ) traveling through the medium [71].

$$I = (\Delta p)/(\Delta v) \quad (5)$$

Using a medium with a low mechanical impedance (such as air) between two mediums with high impedance values (such as steel) attenuates the peak value of the transmitted overpressure [72,73]. In this study, an air gap is present in the mitigation system in order to dissipate the pressure wave depending on the mechanical impedance.

### 2.2. Uni-Float Steel Ferry

The Uni-float steel ferry is used for military purposes to accommodate the tank load of the Military Load Capacity (MLC-70). The ferry is composed of sixteen floating pontoons [74]. Figure 2 illustrates the configuration of the steel pontoons used to form the ferry.

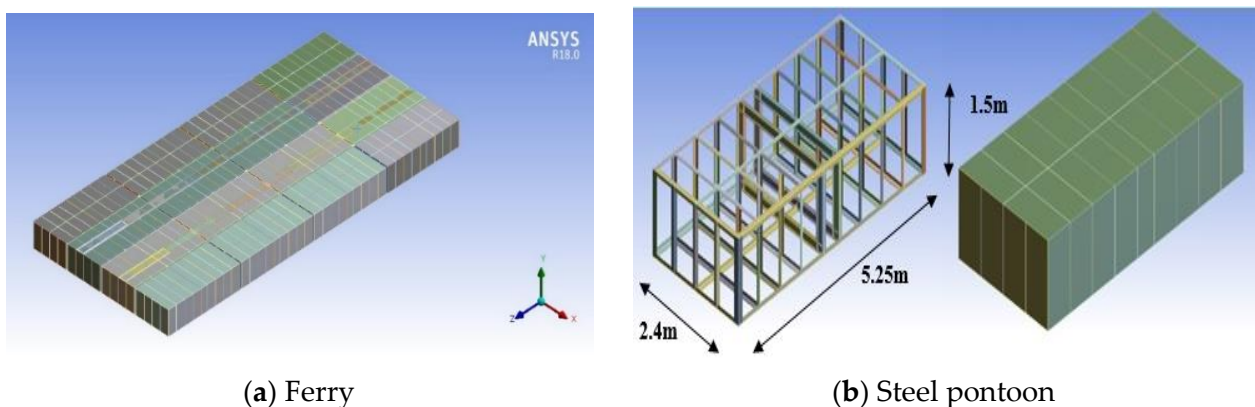


**Figure 2.** Schematic illustrating the ferry and steel pontoon configuration.

Lotfy et al. [65] illustrated the specifications of the floating steel ferry. The properties of the steel used are illustrated in Table 1 [75]. Additionally, a sensitivity analysis is carried out to obtain the sizes of the reasonable elements [65].

**Table 1.** The properties of the used steel (steel 37) [75].

Density	7850 (kg/m <sup>3</sup> )	Erosion factor	1
Shear modulus	8.18 × 10 <sup>10</sup> (G Pa)	Max. eff. strain rate at failure	2.1
Elastic modulus	2.1 × 10 <sup>5</sup> (G Pa)	Thermal softening exponent	1.03
Poisson’s ratio	0.28	Hardening exponent	0.26
Yield stress	2.4 × 10 <sup>5</sup> (kPa)	Melting temperature	1790 (K)
Hardening constant	5.1 × 10 <sup>5</sup> (kPa)	Reference strain rate	1
Strain rate constant	0.014	Bulk modulus	1.59 × 10 <sup>5</sup> (G Pa)

2.3. The Simulation Domain

The commercial software ANSYS AUTODYN 19.0 [76] was used for the numerical simulations and the implementation of the fluid–structure interactions (FSI). The Euler/Lagrange interaction model couples the Eulerian to the Lagrangian structural domain. The domain is defined in Euler solver as a 3D-multi-material. The volume of the domain must be determined according to the experiment’s behavior.

The ferry was simulated, and the boundaries were defined to match realistic conditions, preventing the explosion from being confined; therefore, the boundaries were assigned to a flow-out type in all faces, as shown in Figure 3.

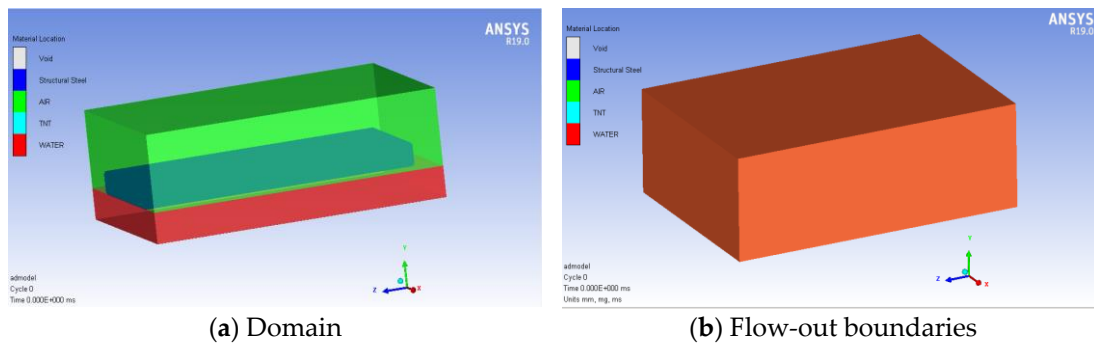


**Figure 3.** The domain and boundaries of the ferry.

The domain was divided into the air (upper side) and water (lower side). The water surfaces were simulated without any boundary due to the effect of the water on the reflection of the pressure wave. The ferry was exposed to explosive charges of Trinitrotoluene (TNT) at a stand-off distance of one meter. The material properties of the air and TNT were retrieved from the standard AUTODYN library. The air part was modeled using 3D Euler equations, while the explosive charge (TNT) was represented according to the Jones Wilkens Lee (JWL) equation of state EOS, with a reference density of 1630 kg/m<sup>3</sup>, according to Equation (6) [31,77,78]:

$$P = C_1 \left(1 - \frac{w}{r_1 v}\right) e^{-r_1 v} + C_2 \left(1 - \frac{w}{r_2 v}\right) e^{-r_2 v} + \frac{we}{v} \tag{6}$$

where “P” indicates the hydrostatic pressure, “v” denotes the specific volume and “e” indicates the specific internal energy, while C<sub>1</sub>, r<sub>1</sub>, C<sub>2</sub>, r<sub>2</sub> and w are the material constants. The values of the constants C<sub>1</sub>, r<sub>1</sub>, C<sub>2</sub>, r<sub>2</sub> and w have been determined for many common explosives from the dynamics. The values of the constants for a TNT explosive are available in AUTODYN, as shown in Table 2 [31,78,79].

**Table 2.** TNT explosive parameters.

Parameters	C1	C2	r1	r2	w
Value	3.7377 × 10 <sup>5</sup> MPa	3.7471 × 10 <sup>3</sup> MPa	4.15	0.9	0.35

In addition, the air is modeled by an ideal gas EOS, which can be expressed as in Equation (7).

$$P = C_1(\gamma - 1)\rho e \tag{7}$$

where “ $\gamma$ ” denotes the heat-specific ratio and “ $\rho$ ” denotes the density. The standard constants of the air were taken from the AUTODYN material library, with an air reference density ( $\rho$ ) equal to 1.225 kg/m<sup>3</sup> and  $\gamma$  equal to 1.4. The initial internal energy of the air is assumed to be  $2.068 \times 10^5$  kJ/kg [78].

The floating pontoons were exposed to side air explosions at a stand-off distance of 1 m and a height of 0.90 m from the bottom of the ferry. This height represents the mid-span of the un-submerged part of the ferry. Global erosion was performed as 1.3 geometric strains; additionally, the global cutoff of the maximum expansion was 0.2. Furthermore, the trajectory interaction between the Lagrangian part and the fully coupled Euler sub-grid and shell elements was performed. Charges of 1 kg, 10 kg, 50 kg and 100 kg were used to study their effect on the ferry in order to determine the maximum side charge that the ferry can withstand. Figure 4 illustrates the charge position for the side explosions. The gauges were installed to determine the displacement of the ferry due to the explosions. Figure 5 illustrates the gauges for the side explosions.

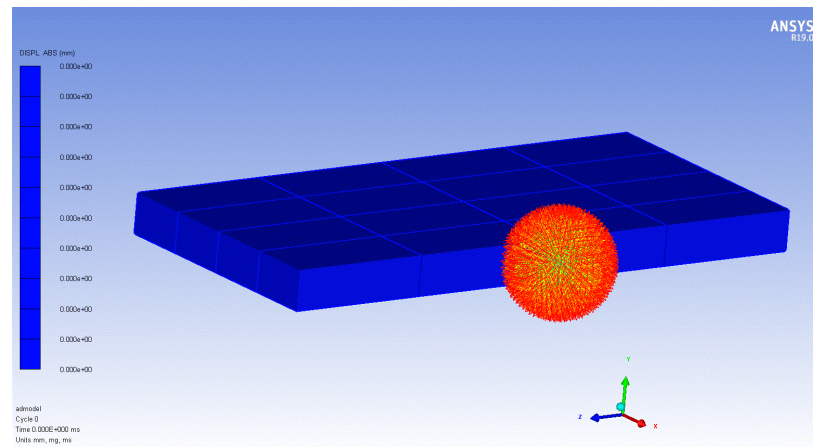


Figure 4. Side explosive charge.

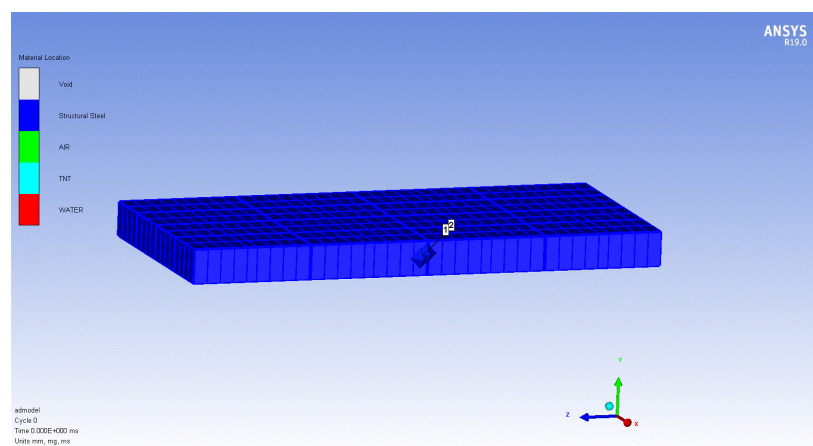


Figure 5. Gauges for the side explosion.

### 3. Validation

Simulating explosion in ANSYS AUTODYN requires the accurate definition of the properties of the used material, the medium that transfers the shock wave, the boundary conditions and the interaction between the different materials. The validation is divided into two parts: First, the validation of the shock wave and the pressure–time history, which affect the materials, and second, the validation of the deformation response of the used material.

#### 3.1. Pressure-Time History

The validation of the pressure–time history depends on both the practical and numerical experiments performed by Fairlie [80]. Fairlie presented a practical example that described the air blast and determined the pressure–time history at the front of a building. Additionally, Fairlie used the scaling law to simulate the test with a scale of 1/50<sup>th</sup>. A small charge of TNT (8 g) is exploded, and the pressure is measured at the elevation of the opposite building. Figure 6 illustrates the physical and numerical experiments.

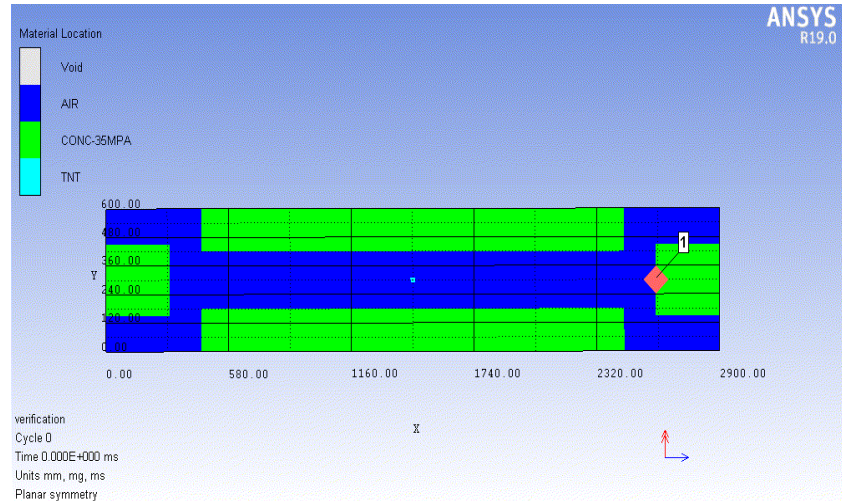
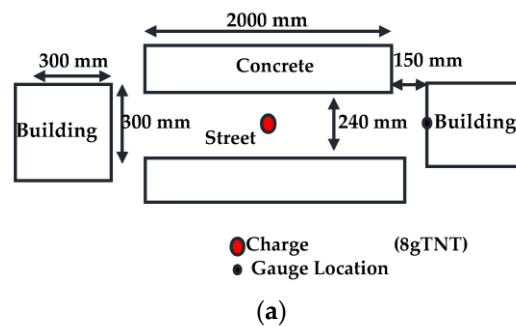


**Figure 6.** Details of the air blast experiment. (a) schematic diagram of the air blast physical [80]. (b) Numerical modelling of the experiment.

The maximum overpressure was measured in the field to be about 380 kPa. The maximum overpressure value from the numerical modeling equals 390 kPa. The matching percentage is 97.4%. Figure 7 illustrates the pressure–time history of both the experimental and numerical results. The pressure–time history curves are similar in both cases. The small changes in the time of arrival between the practical and numerical results are due to the change in the TNT pressure wave velocity.

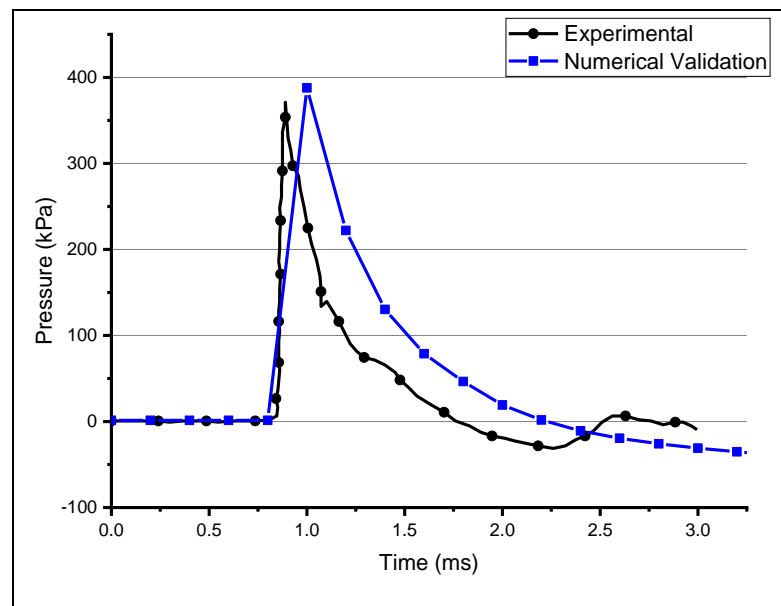


Figure 7. Pressure-time history from simulation and air blast experiment results [80].

### 3.2. Validation Deformation Response

The validation in this section is based on both a real experiment and a series of physical experiments performed by Aune et al. [38]. Aune et al. performed a series of physical experiments and numerical simulations to study the effect of the stand-off distance and the dynamic responses of different materials with different thicknesses. Square steel plate specimens with dimensions of 400 mm × 400 mm × 0.8 mm were tested with a TNT charge of 40.2 gm at different stand-off distances. The verified experiment is mentioned as experiment number S23. Figure 8 illustrates the setup of the experiment.

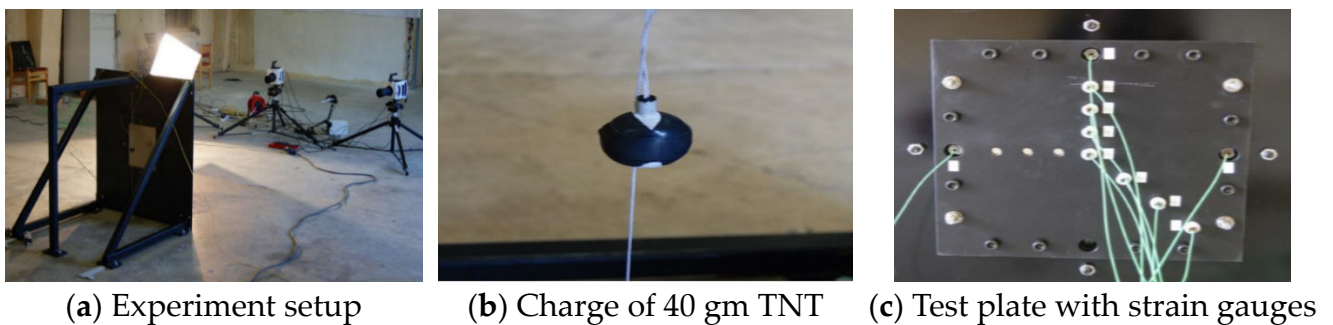
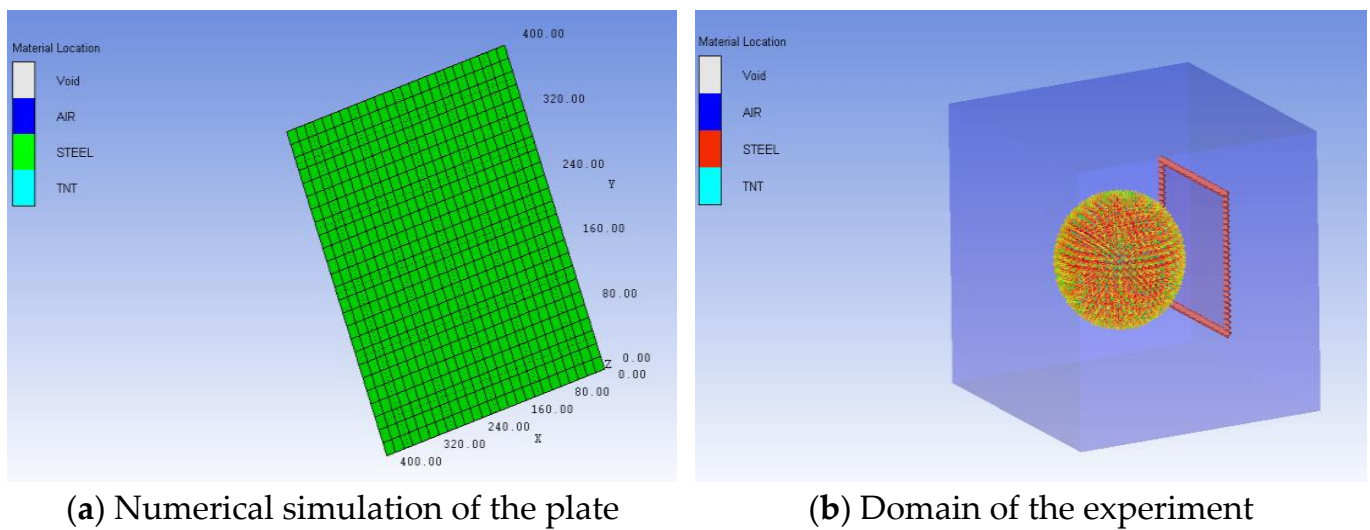


Figure 8. Field experiment [38].

The steel plate was simulated in AUTODYN with the same characteristics as that used in the experiment. The boundary conditions assigned to the plate were the same as the real experiment boundaries. The domain was simulated as an air cube around the plate with flow-out boundaries, which allowed the shockwave to propagate away and prevent its reflection. Figure 9 illustrates the simulated steel plate and the domain with the remapped TNT charge.



**Figure 9.** Blast test simulation.

The obtained deformation value from a spherical charge of 40 gm of TNT with a stand-off distance of 0.25 m equals 18.3 mm, as mentioned in [38]. The maximum numerical displacement value was obtained from the simulation to be 17.4 mm, with a matching percentage of about 95%. Figure 10 illustrates the displacement distribution from the numerical simulation.

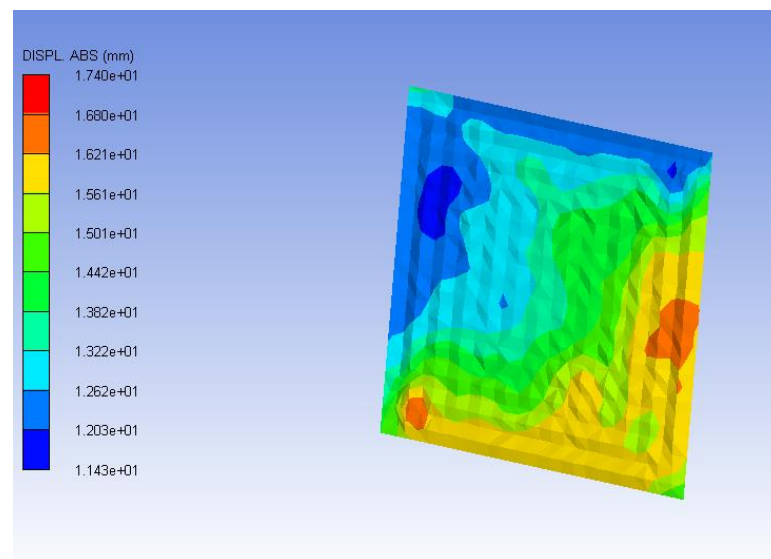


**Figure 10.** Numerical displacement distribution.

#### 4. Side Blast of the Traditional Steel Ferry

The ferry was exposed to the explosion of 5 and 10 kg of TNT sequentially at a stand-off distance of 1 m. The expansion of the side explosion is illustrated in Figure 11. The explosion caused local deformations at the critical positions (in front of the charge).

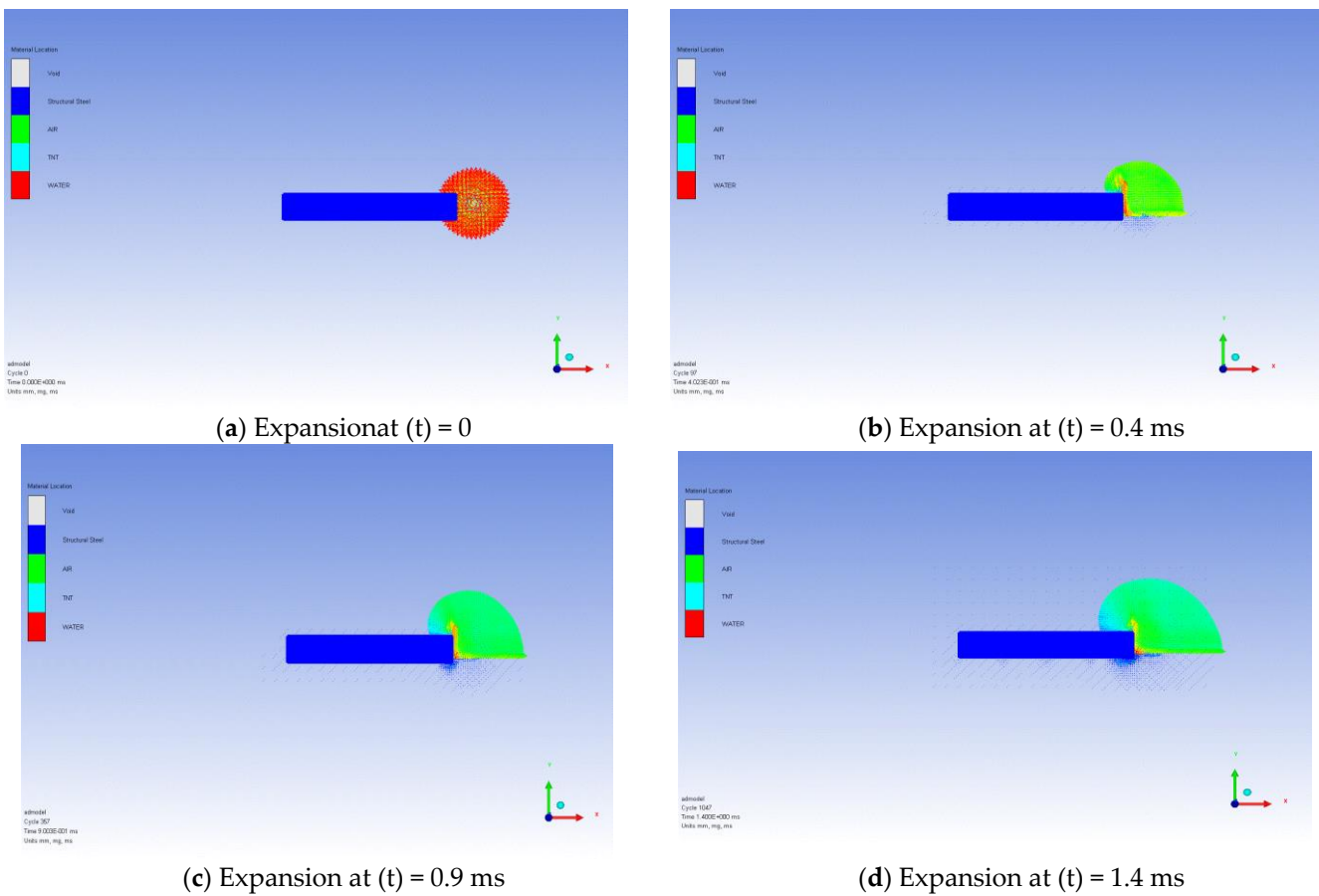


Figure 11. Expansion of the side explosion.

#### 4.1. Results for the Charge 5 kg of TNT

The explosion of a side charge of 5 kg of TNT reveals that there are local deformations at the side shells in addition to the side transition motion of the ferry. The incident pressure wave from the explosion first affects the side shell in a very short rapid time causing local deformations, and then the ferry is affected by this pressure wave. The ferry starts to gain kinetic energy from the explosion, which causes a side translation motion. This translation motion vanishes by the effect of the ferry weight and inertia. Figure 12 illustrates the displacement of the ferry during the explosion. The side translation of the ferry reaches about 8.4 cm, and the material status of the steel remains in the elastic zone.

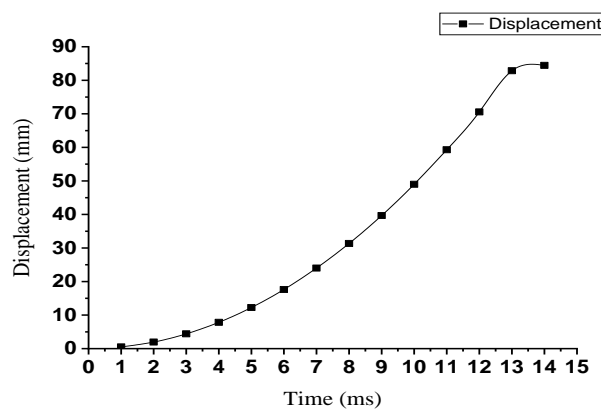
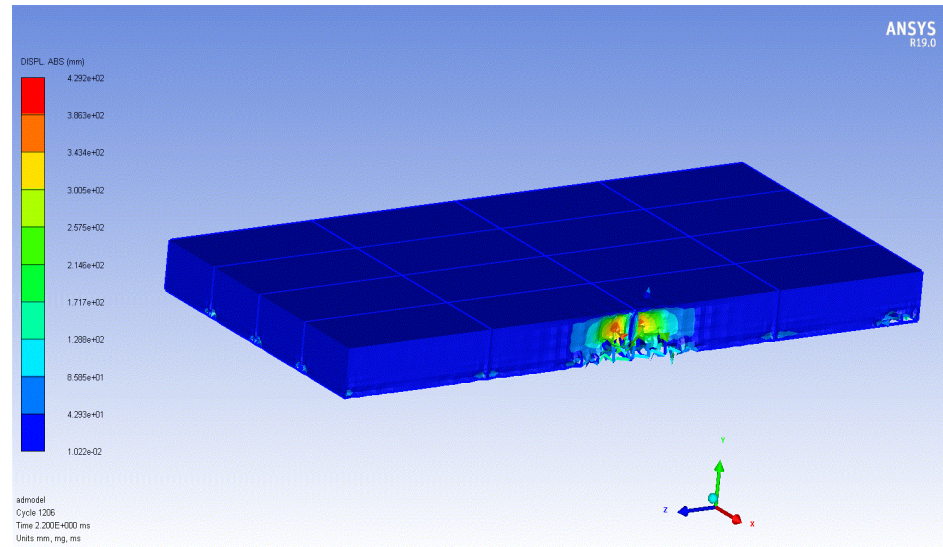


Figure 12. Displacement of the ferry from a side explosion of 5 kg TNT.

#### 4.2. Results for the Charge 10 kg of TNT

The charge is increased to 10 kg of TNT at the same stand-off distance (1 m) to determine the maximum charge that the ferry can withstand. The explosion resulted in excessive local deformations at the critical section (in front of the charge). Figure 13 illustrates the deformed ferry due to the side explosion.



**Figure 13.** Deformations of the ferry.

These local deformations increase until reaching the plastic failure at the lower connection between the side and lower shells. The failure occurs at this section and not at the upper connection because of the increased rigidity in the upper connection between the upper and side shells, as the upper shell's thickness is larger than the lower shell's thickness. Plastic failure occurs at the critical section, while the plastic deformations occur at other lower connections and the side shells around the plastic failure, as illustrated in Figure 14. These deformations illustrate the plastic failure and the erosion of the ferry material.

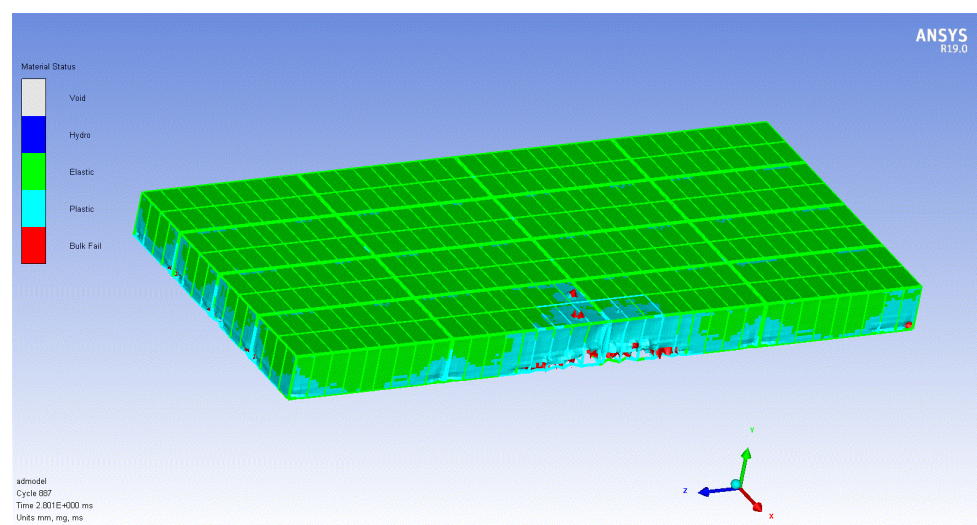


**Figure 14.** Material statuses of the ferry.

The displacement of the ferry from a side explosion due to 10 kg of TNT is illustrated in Figure 15.

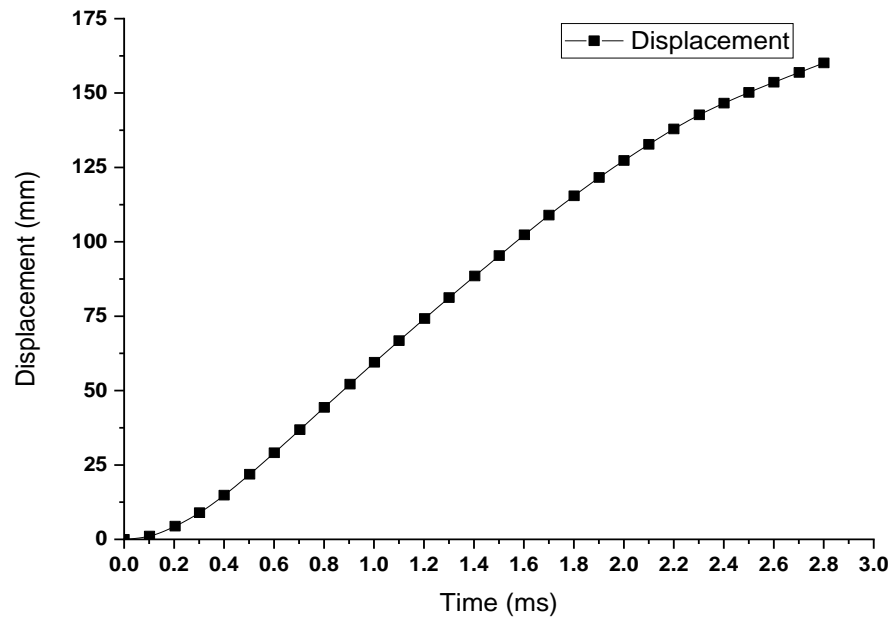


Figure 15. Deformations of the ferry from a side explosion due to 10 kg of TNT.

### 5. Mitigation System

The proposed mitigation system depends on the wave impedance by using an air gap, which results in the dissipation of the pressure wave; additionally, the shape of the mitigation system greatly affects the dissipation of the pressure wave. The proposed structure is a panel composed of a curved steel surface with internal stiffeners. Every panel is connected to the side of the pontoon. This panel weighs 270 kg, which is very low in comparison to the pontoon’s weight (3.6 t). These panels are only added to the right and left sides of the ferry. Figure 16 illustrates the proposed mitigation system. This mitigation panel has internal stiffeners in order to increase the stiffness of the structure to withstand the explosive charge and increase the capacity against lateral buckling, as shown in Figure 17.

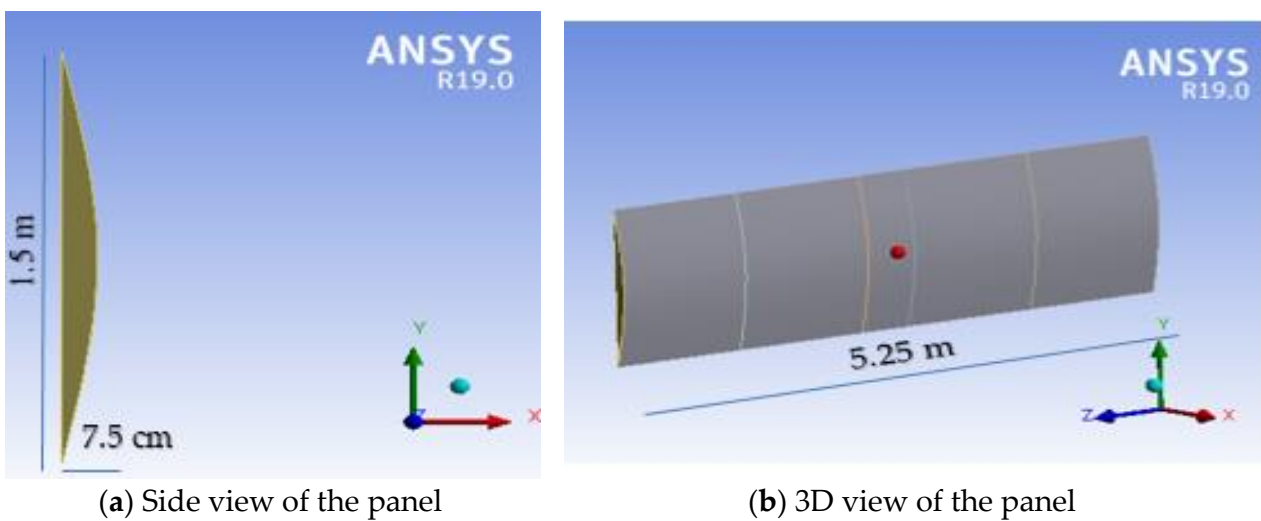
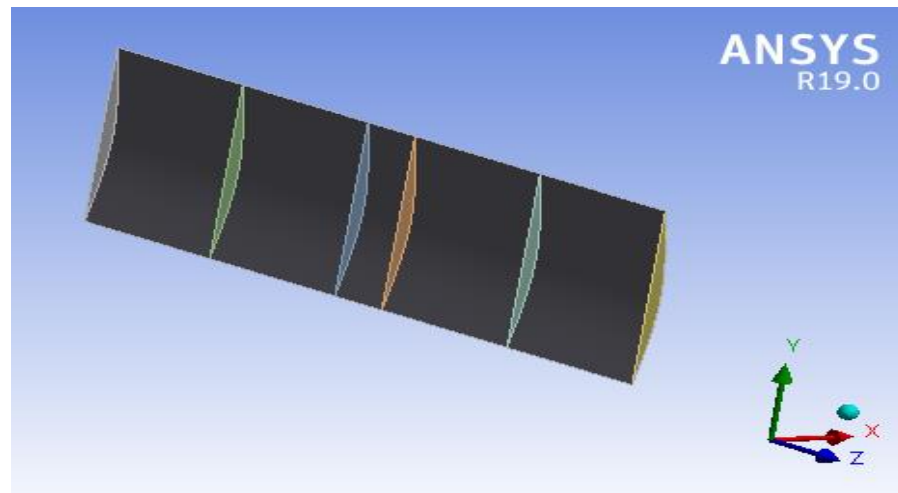
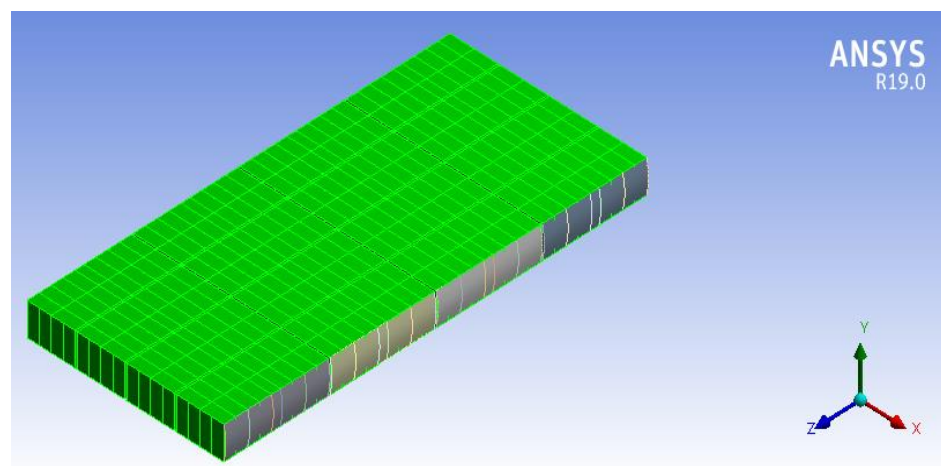


Figure 16. Mitigation panel.



**Figure 17.** Internal stiffeners arrangement.

These mitigation panels are installed on two sides of the steel ferry (four panels on each side). The internal spaces between the panels and the pontoons are used as air gaps, which is the basis for using the scientific theory of impedance. Figure 18 illustrates the mitigation panels on one side of the steel ferry. The ferry is still stable on both sides after installing the mitigation panels due to the symmetry.



**Figure 18.** Mitigation panels at the side of the steel ferry.

### 5.1. Ferry Stability

The ferry is still stable after the installation of these new panels, whereas the centroid of the ferry is the same as before (without mitigation panels). The ferry weight is increased by about 2.15 t, but the volume of the ferry is increased, which results in almost the same values as the draft.

### 5.2. Side Blast Results

The fortified ferry was exposed to the same charge as the previous case (10 kg of TNT at a stand-off distance of 1 m). Figure 19 illustrates the material condition of the ferry with the new mitigation system after the explosion of the charge.

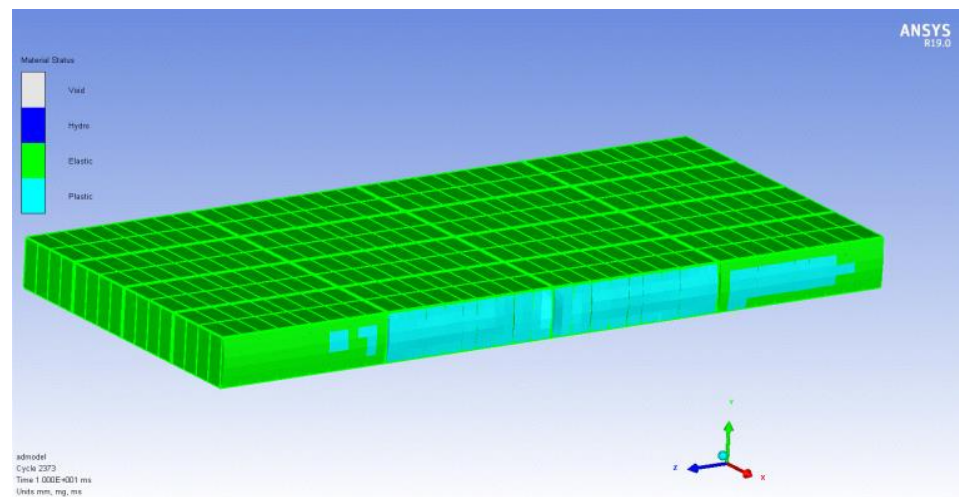


**Figure 19.** Deformations on the mitigation panels.

The mitigation system was found to dissipate the blast waves and reduce the effect of the explosion. The blast waves were divided into incident waves, diffracted waves and dissipated waves, which were successfully dissipated by the mitigation system.

The ferry can resist the charge without any plastic failure in the pontoons or even in the mitigation system. The installed panels are exposed to plastic deformations, while the pontoons of the ferry are not exposed to any plastic deformations or plastic failure. The effects of the explosion on the pontoons and the mitigation panels are illustrated in Figure 20.

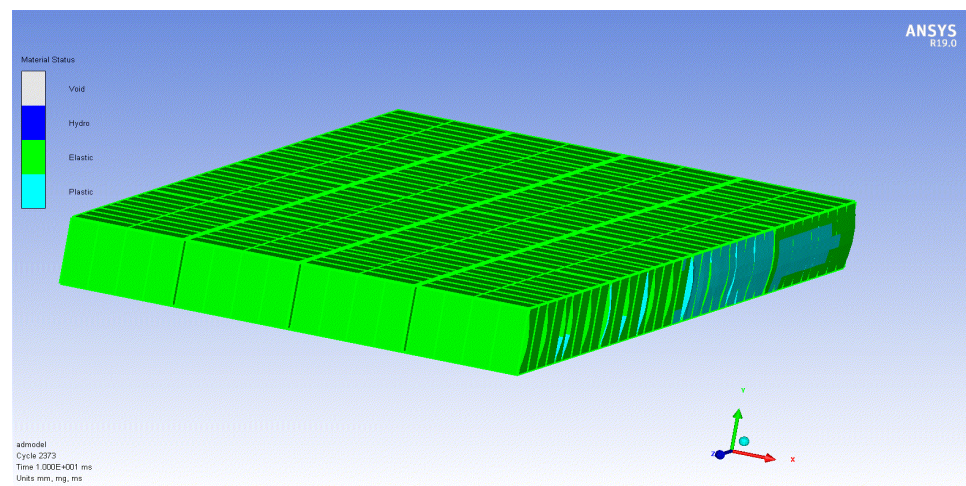


**Figure 20.** Material statuses beyond the mitigation system.

Plastic deformations only occurred at the stiffener's positions of the mitigation panels and not in the steel pontoons. The deformations of the fortified ferry corresponding to the explosion are illustrated in Figure 21.

The maximum value of the total deformations was found to be 6.9 cm, which is lower than the used curvature of the mitigation panel (7.5 cm). Figure 22 illustrates the response of the floating ferry subjected to an explosion of 10 kg of TNT after installing the mitigation system.

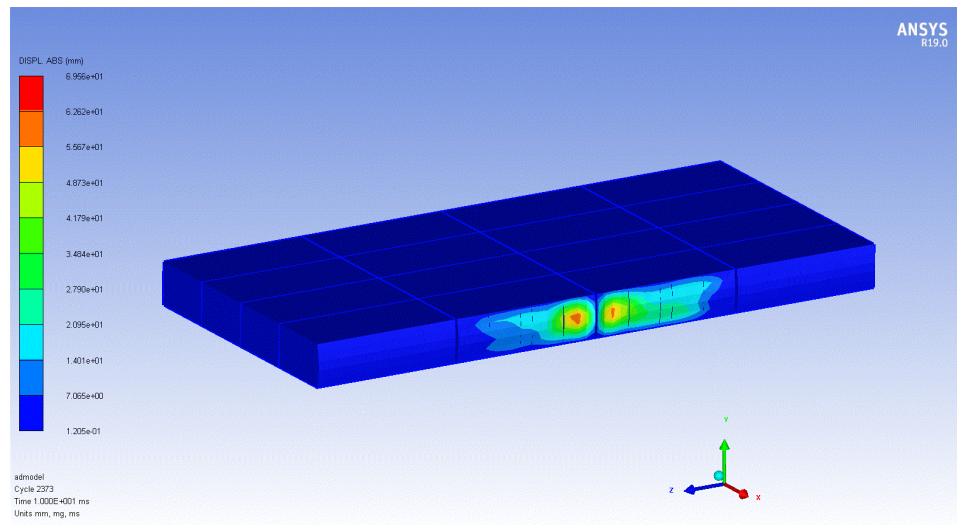
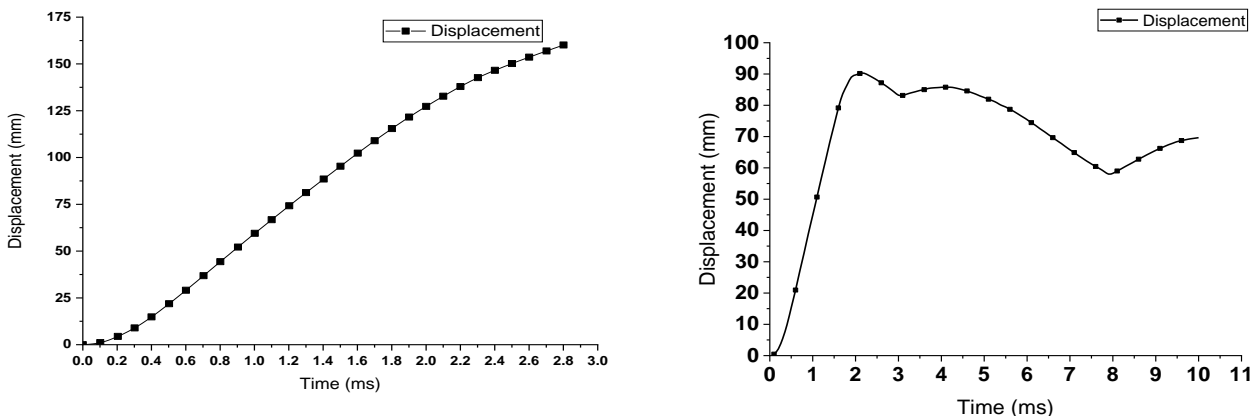


Figure 21. Total deformations of the fortified ferry.



(a) Displacement time history without the mitigation system (b) Displacement time history with the mitigation system

Figure 22. The displacement response.

The maximum displacement occurs at the side shell of the ferry behind the mitigation system. The maximum deformation at the critical section behind the mitigation system equals about 8.8 cm. This deformation value occurs as a combination of the transitional movement of the ferry and the local deformations of the critical section. As a result, the ferry moved transversely in the water by about 6 cm, while the local deformations reached about 2.8 cm.

### 6. Conclusions

This paper presents the results of numerical analyses on steel floating pontoons exposed to side explosions with different explosive charges to achieve a design that can sustain the blast loads with minimal deformations. The fluid–structure interactions with the air and water were simulated using ANSYS AUTODYN 19.0. The ferry hull was analyzed under an explosion of 5 kg and 10 kg of TNT. For the charge of 5 kg of TNT, the maximum displacement was found to be about 8.4 cm with the elastic behavior of the ferry material, while the ferry is damaged under the explosion of 10 kg of TNT. An innovative mitigation system was proposed to resist explosion attacks from terrorists or conventional bombs. The proposed mitigation system is composed of separated mitigation steel panels. These panels increase the capacity of the floating steel ferry to withstand explosive charges until a charge of 10 kg of TNT at a stand-off distance of 1 m, while the original ferry could not withstand this charge. The mitigation panels are capable of

reducing the deformation and impulse transmitted to the base structure. The maximum displacement from the explosion of 10 kg of TNT after using the mitigation panels reaches about 8.8 cm. It has been found that the mitigation system dissipates the pressure wave by using the air gap between the original pontoons and the proposed panels. The presented mitigation system showed outstanding blast wave mitigation capabilities. The results showed that the mitigation system could mitigate more than 50% of the blast waves with almost full protection for the targeted structure. Such success can only be attributed to its exceptional design. Furthermore, ANSYS AUTODYN demonstrated a great capability in studying air–water–structural interactions with a good level of accuracy.

**Author Contributions:** Conceptualization, E.F. and Y.A.K.; Formal analysis, E.F. and M.N.L.; Funding acquisition, E.F., Y.A.K. and M.N.L.; Methodology, E.F. and Y.A.K.; Resources, E.F. and Y.A.K.; Software, E.F. and M.N.L.; Supervision, E.F. and Y.A.K.; Writing—original draft, E.F., M.N.L. and Y.A.K.; Writing—review and editing, E.F. and Y.A.K. All authors have read and agreed to the published version of the manuscript.

**Funding:** This research received no external funding.

**Institutional Review Board Statement:** Not applicable.

**Informed Consent Statement:** Not applicable.

**Data Availability Statement:** The data presented in this study are all included in this article.

**Acknowledgments:** The authors are thankful to Military Technical College (Cairo, Egypt) for providing all the necessary facilities to carry out that research.

**Conflicts of Interest:** The authors declare no conflict of interest.

## References

1. Abbas, A.; Adil, M.; Ahmad, N.; Ahmad, I. Behavior of reinforced concrete sandwiched panels (RCSPs) under blast load. *Eng. Struct.* **2019**, *181*, 476–490. [[CrossRef](#)]
2. Draganić, H.; Gazić, G.; Varevac, D. Experimental investigation of design and retrofit methods for blast load mitigation—A state-of-the-art review. *Eng. Struct.* **2019**, *190*, 189–209. [[CrossRef](#)]
3. Li, Z.; Chen, W.; Hao, H. Numerical study of sandwich panel with a new bi-directional Load-Self-Cancelling (LSC) core under blast loading. *Thin-Walled Struct.* **2018**, *127*, 90–101. [[CrossRef](#)]
4. Helal, M.M.; Elsayed, F.J.M.T. Dynamic behavior of stiffened plates under underwater shock loading. *Mater. Test.* **2015**, *57*, 506–517. [[CrossRef](#)]
5. Fathallah, E.; Qi, H.; Tong, L.; Helal, M. Numerical Simulation and Response of Stiffened Plates Subjected to Non-Contact Underwater Explosion. *Adv. Mater. Sci. Eng.* **2014**, *2014*, 1–18. [[CrossRef](#)]
6. Fathallah, E.; Qi, H.; Tong, L.; Helal, M. Numerical investigation of the dynamic response of optimized composite elliptical submersible pressure hull subjected to non-contact underwater explosion. *Compos. Struct.* **2015**, *121*, 121–133. [[CrossRef](#)]
7. Xu, J.; Liu, J.; Gu, W.; Liu, X.; Cao, T. Shock Wave Attenuation Characteristics of Aluminum Foam Sandwich Panels Subjected to Blast Loading. *Shock. Vib.* **2018**, *2018*, 1–10. [[CrossRef](#)]
8. Helal, M.; Huang, H.; Fathallah, E.; Wang, D.; ElShafey, M.M.; Ali, M.A.E.M. Numerical Analysis and Dynamic Response of Optimized Composite Cross Elliptical Pressure Hull Subject to Non-Contact Underwater Blast Loading. *Appl. Sci.* **2019**, *9*, 3489. [[CrossRef](#)]
9. Elsayed, F.; Nagy, N.M.; Lili, T. Numerical Evaluation of Composite Plates Performance under the Effect of Underwater Explosion. In Proceedings of the 15th International Conference on Aerospace Sciences & Aviation Technology, Cairo, Egypt, 28–30 May 2013; pp. 1–15.
10. Liu, H.; Cao, Z.K.; Yao, G.C.; Luo, H.J.; Zu, G.Y. Performance of aluminum foam–steel panel sandwich composites subjected to blast loading. *Mater. Des.* **2013**, *47*, 483–488. [[CrossRef](#)]
11. Wang, C.; Xu, B.; Yuen, S.C.K. Numerical analysis of cladding sandwich panels with tubular cores subjected to uniform blast load. *Int. J. Impact Eng.* **2019**, *133*, 103345. [[CrossRef](#)]
12. Chen, D.; Jing, L.; Yang, F. Optimal design of sandwich panels with layered-gradient aluminum foam cores under air-blast loading. *Compos. Part B Eng.* **2019**, *166*, 169–186. [[CrossRef](#)]
13. Wang, Y.; Wang, H.; Cui, C.; Zhao, B. Investigating Different Grounds Effects on Shock Wave Propagation Resulting from Near-Ground Explosion. *Appl. Sci.* **2019**, *9*, 3639. [[CrossRef](#)]
14. Zhou, X.Q.; Hao, H. Prediction of airblast loads on structures behind a protective barrier. *Int. J. Impact Eng.* **2008**, *35*, 363–375. [[CrossRef](#)]

15. Wahab, M.M.A.; Mazek, S.; Abada, M.M.; Atta, M.H.A. Effect of blast wave on lightweight structure performance. *J. Eng. Sci. Mil. Technol.* **2017**, *1*, 1–6. [[CrossRef](#)]
16. Alqwasmī, N.; Tarlochan, F.; Alkhatib, E.S. Study of Mild Steel Sandwich Structure Energy Absorption Performance Subjected to Localized Impulsive Loading. *Materials* **2020**, *13*, 670. [[CrossRef](#)]
17. Alogla, A.; Helal, M.; ElShafey, M.M.; Fathallah, E. Numerical Analysis for Critical Structures Protection against Blast Loading Using Metallic Panels. *Appl. Sci.* **2020**, *10*, 2121. [[CrossRef](#)]
18. Markose, A.; Rao, C.L. *Effectiveness of Polyurea Coated Steel Plates in Blast Mitigation in Vehicles*; Springer: Singapore, 2020; pp. 153–164.
19. Esa, M.; Amin, M.S.; Hassan, A. Relative performance of novel blast wave mitigation system to conventional system based on mitigation percent criteria. *Def. Technol.* **2021**, *17*, 912–922. [[CrossRef](#)]
20. Jin, M.; Hao, Y.; Hao, H. Numerical study of fence type blast walls for blast load mitigation. *Int. J. Impact Eng.* **2019**, *131*, 238–255. [[CrossRef](#)]
21. Zhou, H.; Zhang, X.; Wang, X.; Du, X.; Yu, S.; Wang, Y. Jiang Protection effectiveness of sacrificial cladding for near-field blast mitigation. *Int. J. Impact Eng.* **2022**, *170*, 104361. [[CrossRef](#)]
22. Khalifa, Y.A.; Campidelli, M.; Tait, M.J.; El-Dakhkhni, W.W. Mitigating Risk of Confined Explosion via Lightweight Sacrificial Cladding. *J. Perform. Constr. Facil.* **2020**, *34*, 04019080. [[CrossRef](#)]
23. Langdon, G.S.; Karagiozova, D.; Theobald, M.D.; Nurick, G.N.; Lu, G.; Merrett, R. Fracture of aluminium foam core sacrificial cladding subjected to air-blast loading. *Int. J. Impact Eng.* **2010**, *37*, 638–651. [[CrossRef](#)]
24. Ousji, H.; Belkassem, B.; Louar, M.A.; Reymen, B.; Martino, J.; Lecompte, D.; Pyl, L.; Vantomme, J. Air-blast response of sacrificial cladding using low density foams: Experimental and analytical approach. *Int. J. Mech. Sci.* **2017**, *128*, 459–474. [[CrossRef](#)]
25. Zhang, L.; Hebert, R.; Wright, J.T.; Shukla, A.; Kim, J.-H. Dynamic response of corrugated sandwich steel plates with graded cores. *Int. J. Impact Eng.* **2014**, *65*, 185–194. [[CrossRef](#)]
26. Britan, A.; Liverts, M.; Shapiro, H.; Ben-Dor, G. Blast Wave Mitigation by a Particulate Foam Barrier. *Transp. Porous Media* **2012**, *93*, 283–292. [[CrossRef](#)]
27. Taha, A.K.; Gao, Z.; Dahai, H.; Zahran, M.S. Response of a new structural ultra-high performance concrete barrier wall subjected to blast loading. *Aust. J. Struct. Eng.* **2020**, *21*, 154–161. [[CrossRef](#)]
28. Peña, M.E.C. Blast Loading Retrofit of Unreinforced Masonry Walls. *Struct. Perform. Mag.* **2009**, 16–20.
29. McDonald, B.; Bornstein, H.; Langdon, G.; Curry, R.; Daliri, A.; Orifici, A. Experimental response of high strength steels to localised blast loading. *Int. J. Impact Eng.* **2018**, *115*, 106–119. [[CrossRef](#)]
30. Sun, G.; Wang, E.; Zhang, J.; Li, S.; Zhang, Y.; Li, Q. Experimental study on the dynamic responses of foam sandwich panels with different facesheets and core gradients subjected to blast impulse. *Int. J. Impact Eng.* **2019**, *135*, 103327. [[CrossRef](#)]
31. Zong, R.; Hao, H.; Shi, Y. Development of a New Fence Type Blast Wall for Blast Protection: Numerical Analysis. *Int. J. Struct. Stab. Dyn.* **2017**, *17*, 1–29. [[CrossRef](#)]
32. Xia, Y.; Wu, C.; Zhang, F.; Li, Z.-X.; Bennett, T. Numerical Analysis of Foam-Protected RC Members under Blast Loads. *Int. J. Prot. Struct.* **2014**, *5*, 367–390. [[CrossRef](#)]
33. Wu, C.; Sheikh, H. A finite element modelling to investigate the mitigation of blast effects on reinforced concrete panel using foam cladding. *Int. J. Impact Eng.* **2013**, *55*, 24–33. [[CrossRef](#)]
34. Yazici, M.; Wright, J.; Bertin, D.; Shukla, A. Experimental and numerical study of foam filled corrugated core steel sandwich structures subjected to blast loading. *Compos. Struct.* **2014**, *110*, 98–109. [[CrossRef](#)]
35. Wahab, M.A.; Mazek, S.; Abada, M.; Shafy, M.A. Blast hazard impact on V-shape composite panel performance. *J. Eng. Sci. Mil. Technol.* **2018**, *2*, 90–99. [[CrossRef](#)]
36. Walkowiak, M.; Reinicke, U.; Anders, D. Numerical Investigation of Different Core Topologies in Sandwich-Structured Composites Subjected to Air-Blast Impact. *Appl. Sci.* **2022**, *12*, 9012. [[CrossRef](#)]
37. Lin, H.; Han, C.; Yang, L.; Zhang, L.; Luan, H.; Han, X.; Zhang, S. Numerical Investigation on Performance Optimization of Offshore Sandwich Blast Walls with Different Honeycomb Cores Subjected to Blast Loading. *J. Mar. Sci. Eng.* **2022**, *10*, 1743. [[CrossRef](#)]
38. Aune, V.; Fagerholt, E.; Hauge, K.O.; Langseth, M.; Børvik, T. Experimental study on the response of thin aluminium and steel plates subjected to airblast loading. *Int. J. Impact Eng.* **2016**, *90*, 106–121. [[CrossRef](#)]
39. Smith; Hetherington, J. *Blast and Ballistic Loading of Structures*, 1st ed.; Laxton's Publishing: Oxford, UK, 1994.
40. Martin, R.J.; Reza, A.; Anderson, L.W. What is an explosion? A case history of an investigation for the insurance industry. *J. Loss Prev. Process Ind.* **2000**, *13*, 491–497. [[CrossRef](#)]
41. Needham, C.E. *Blast Waves*; Springer: Berlin/Heidelberg, Germany, 2010; Volume 402.
42. Yuen, S.C.K.; Nurick, G.; Verster, W.; Jacob, N.; Vara, A.; Balden, V.; Bwalya, D.; Govender, R.; Pittermann, M. Deformation of mild steel plates subjected to large-scale explosions. *Int. J. Impact Eng.* **2008**, *35*, 684–703. [[CrossRef](#)]
43. Parviz, M.; Aminnejad, B.; Fiouz, A. Numerical simulation of dynamic response of water in buried pipeline under explosion. *KSCE J. Civ. Eng.* **2017**, *21*, 2798–2806. [[CrossRef](#)]
44. Caçoilo, A.; Mourão, R.; Belkassem, B.; Teixeira-Dias, F.; Vantomme, J.; Lecompte, D. Blast Wave Assessment in a Compound Survival Container: Small-Scale Testing. *Multidiscip. Digit. Publ. Inst. Proc.* **2018**, *2*, 540.

45. Bajić, Z.; Bogdanov, J.; Dimitrijević, R.; Jeremić, R. Investigation of Scaled Distance Influence on Shockwave Overpressure for Plastic Explosive PPE-01. In Proceedings of the 19th Seminar on New Trends in Research of Energetic Materials (NTREM), Pardubice, Czech Republic, 20–22 April 2016; pp. 361–396.
46. Goswami, A.; Adhikary, S.D. Retrofitting materials for enhanced blast performance of Structures: Recent advancement and challenges ahead. *Constr. Build. Mater.* **2019**, *204*, 224–243. [[CrossRef](#)]
47. Draganić, H.; Sigmund, V. Blast loading on structures. *Tech. Gaz.* **2012**, *19*, 643–652.
48. Iqbal, J. *Effects of an External Explosion on a Concrete Structure*; University of Engineering and Technology: Lahore, Pakistan, 2009.
49. Cooper, W. *Explosives Engineering*; John Wiley & Sons: New York, NY, USA, 2018.
50. Simmons, M.; Schleyer, G. Pulse pressure loading of aircraft structural panels. *Thin-Walled Struct.* **2006**, *44*, 496–506. [[CrossRef](#)]
51. Bulson, S. *Explosive Loading of Engineering Structures*; CRC Press: Boca Raton, FL, USA, 1997.
52. Hashmi, M. Strain rate sensitivity of a mild steel at room temperature and strain rates of up to  $105 \text{ s}^{-1}$ . *J. Strain Anal. Eng. Des.* **1980**, *15*, 201–207. [[CrossRef](#)]
53. Marsh, K.; Campbell, J. The effect of strain rate on the post-yield flow of mild steel. *J. Mech. Phys. Solids* **1963**, *11*, 49–63. [[CrossRef](#)]
54. Samanta, S.K. Resistance to dynamic compression of low-carbon steel and alloy steels at elevated temperatures and at high strain-rates. *Int. J. Mech. Sci.* **1968**, *10*, 613–636. [[CrossRef](#)]
55. Zener, C.; Hollomon, J.H. Effect of strain rate upon plastic flow of steel. *J. Appl. Phys.* **1944**, *15*, 22–32. [[CrossRef](#)]
56. NagarajaRao, N.; Lohrmann, M.; Tall, L. Effect of strain rate on the yield stress of structural steel. *ASTM J. Mater.* **1966**, *1*, 1–54.
57. Sen, S.; Banerjee, B.; Shaw, A. Taylor impact test revisited: Determination of plasticity parameters for metals at high strain rate. *Int. J. Solids Struct.* **2020**, *193*, 357–374. [[CrossRef](#)]
58. Koerber, H.; Xavier, J.; Camanho, P.P. High strain rate characterisation of unidirectional carbon-epoxy IM7-8552 in transverse compression and in-plane shear using digital image correlation. *Mech. Mater.* **2010**, *42*, 1004–1019. [[CrossRef](#)]
59. Grażka, M.; Janiszewski, J. Identification of Johnson–Cook equation constants using finite element method. *Eng. Trans.* **2012**, *60*, 215–223.
60. *ANSYS Autodyn User’s Manual (Release 15.0)*; ANSYS, Inc.: Canonsburg, PA, USA, 2013.
61. Dorogoy, A.; Rittel, D. Determination of the Johnson–Cook material parameters using the SCS specimen. *Exp. Mech.* **2009**, *49*, 881. [[CrossRef](#)]
62. Milani, A.; Dabboussi, W.; Nemes, J.A.; Abeyaratne, R. An improved multi-objective identification of Johnson–Cook material parameters. *Int. J. Impact Eng.* **2009**, *36*, 294–302. [[CrossRef](#)]
63. Banerjee, A.; Dhar, S.; Acharyya, S.; Datta, D.; Nayak, N. Determination of Johnson cook material and failure model constants and numerical modelling of Charpy impact test of armour steel. *Mater. Sci. Eng. A* **2015**, *640*, 200–209. [[CrossRef](#)]
64. Wang, X.; Shi, J. Validation of Johnson–Cook plasticity and damage model using impact experiment. *Int. J. Impact Eng.* **2013**, *60*, 67–75. [[CrossRef](#)]
65. Lotfy, M.N.; Khalifa, Y.A.; Dessouki, A.K.; Fathallah, E. Dynamic Behavior of Steel and Composite Ferry Subjected to Transverse Eccentric Moving Load Using Finite Element Analysis. *Appl. Sci.* **2020**, *10*, 5367. [[CrossRef](#)]
66. Lotfy, M.; Fathallah, E.; Khalifa, Y.; Dessouki, A. Simulation and Optimization of a CFRP and a GFRP floating pontoon. *IOP Conf. Ser. Mater. Sci. Eng.* **2020**, *934*, 012037. [[CrossRef](#)]
67. Levinson, E.; Horst, J.T.; Willcocks, M. The next generation marine inertial navigator is here now. In Proceedings of the 1994 IEEE Position, Location and Navigation Symposium-PLANS’94, Las Vegas, NV, USA, 11–15 April 1994; pp. 121–127.
68. Gold, S. Military biometrics on the frontline. *Biom. Technol. Today* **2010**, *2010*, 7–9. [[CrossRef](#)]
69. US Army Engineer Waterways Experiment Station. TM5-855-1 Fundamentals of Protective Design for Conventional Weapons. In *US Army, Navy and Air Force*; US Government Printing Office: Washington, WA, USA, 1986.
70. Ma, G.; Ye, Z. Energy absorption of double-layer foam cladding for blast alleviation. *Int. J. Impact Eng.* **2007**, *34*, 329–347. [[CrossRef](#)]
71. Mahmoud, M.M.; Mahfouz, S.Y.; Farag, H.M. Effect of air gap on the structural response of aluminum foam protected reinforced concrete panels. *Int. Conf. Civ. Archit. Eng.* **2018**, *12*, 1–13. [[CrossRef](#)]
72. Cooper, G. Protection of the lung from blast overpressure by thoracic stress wave decouplers. *J. Trauma Acute Care Surg.* **1996**, *40*, 105S–110S. [[CrossRef](#)]
73. Tan, P.; Lee, B.; Tsangalis, C. FEA modelling prediction of the transmitted overpressure and particle acceleration within a frame subjected to shock tube blast loadings. In Proceedings of the 18th World IMACS/MODSIM Congress, Cairns, Australia, 13–17 July 2009.
74. Lotfy, M.N.; Khalifa, Y.A.; Fathallah, E. Simulation and Optimization of a Metallic Ferry under MLC70 Loading. *IOP Conf. Ser. Mater. Sci. Eng.* **2020**, *974*, 012008. [[CrossRef](#)]
75. Rashed, A.; Yazdani, M.; Babaluo, A.; Parvin, H. Investigation on high-velocity impact performance of multi-layered alumina ceramic armors with polymeric interlayers. *J. Compos. Mater.* **2016**, *50*, 3561–3576. [[CrossRef](#)]
76. ANSYS, Inc. *Products Release 19.0*; ANSYS, Inc.: Canonsburg, PA, USA, 2019.
77. Fedorova, N.; Valger, S.; Fedorov, A. Simulation of blast action on civil structures using ANSYS Autodyn. *AIP Conf. Proc.* **2016**, *1770*, 020016.
78. Zheng, C.; Kong, X.-S.; Wu, W.-G.; Xu, S.-X.; Guan, Z.-W. Experimental and numerical studies on the dynamic response of steel plates subjected to confined blast loading. *Int. J. Impact Eng.* **2018**, *113*, 144–160. [[CrossRef](#)]

79. Wu, C.; Lu, Y.; Hao, H. Numerical prediction of blast-induced stress wave from large-scale underground explosion. *Int. J. Numer. Anal. Methods Geomech.* **2004**, *28*, 93–109. [[CrossRef](#)]
80. Fairlie, G. The numerical simulation of high explosives using AUTODYN-2D & 3D. In *Institute of Explosive Engineers 4th Biannual Symposium*; 1998; pp. 743–751. Available online: <http://www.truegrid.com/paper052f.pdf> (accessed on 1 December 2022).

**Disclaimer/Publisher’s Note:** The statements, opinions and data contained in all publications are solely those of the individual author(s) and contributor(s) and not of MDPI and/or the editor(s). MDPI and/or the editor(s) disclaim responsibility for any injury to people or property resulting from any ideas, methods, instructions or products referred to in the content.